Research Square

Preprints are preliminary reports that have not undergone peer review.
They should not be considered conclusive, used to inform clinical practice,
or referenced by the media as validated information.

A minimal delay-programmed model unifying kinetic-chain timing and stretch--shortening-cycle enhancement in tennis racket acceleration

Sun-Hyun Youn

sunyoun@jnu.ac.kr

Chonnam National University

Research Article

Keywords: tennis biomechanics, kinetic chain, stretch–shortening cycle, release delay, active stiffness, reduced-order model

Posted Date: November 6th, 2026

DOI: https://doi.org/10.21203/rs.3.rs-10798450/v1

License: This work is licensed under a Creative Commons Attribution 4.0 International License.
Read Full License

Additional Declarations: No competing interests reported.

A minimal delay-programmed model unifying kinetic-chain timing and stretch–shortening-cycle enhancement in tennis racket acceleration

Sun-Hyun Youn[1*]

[1*] Department of Physics, Chonnam National University, Gwangju, 500-757, Korea .

Corresponding author(s). E-mail(s): sunyoun@jnu.ac.kr;

Abstract

The stretch–shortening cycle (SSC) is among the best-documented mechanisms of enhanced power output in striking skills, yet it emerges from a complex interplay of tendon recoil, pre-activation, and reflex action that is difficult to embed in the simple mechanical models commonly used in racket-sport engineering. We present a minimal planar body–arm–racket model in which (i) each joint stores elastic energy in a latched posture and is released after an explicitly programmed delay, and (ii) the shoulder and wrist may additionally engage a reduced SSC whose active character is captured by only two parameters: a rebound stiffness gain $\boldsymbol{\alpha}$ and a velocity-dependent firing gain $\boldsymbol{\beta}$. Because both mechanisms enter the equations of motion through the same joint-torque algorithm, kinetic-chain timing and SSC enhancement can be optimized within a single computational framework. With optimally tuned delays, racket-tip speed grows superadditively from $16.6\,\mathrm{m\,s^{-1}}$ (one active joint) to $30.2\,\mathrm{m\,s^{-1}}$ (two joints) and $43.1\,\mathrm{m\,s^{-1}}$ (three joints); engaging the SSC within the same firing schedule raises the peak to $46.7\,\mathrm{m\,s^{-1}}$ ($\boldsymbol{\approx 8\%}$), at essentially the same impact frame. The model thus provides a drop-in, analytically transparent surrogate for muscle-level simulation of racket strokes.

Keywords: tennis biomechanics, kinetic chain, stretch–shortening cycle, release delay, active stiffness, reduced-order model

1 Introduction

High racket-head speed at ball contact is one of the principal mechanical determinants of stroke performance in tennis. In a powerful serve or forehand drive the racket is not accelerated by wrist action alone: motion originates in the large proximal segments, propagates through the trunk and shoulder, and reaches the racket only after a delayed distal release. This proximal-to-distal organization, commonly termed the kinetic chain, has been documented across a wide range of striking and throwing skills [1–5]. A second, equally well-established contributor to stroke power is the stretch–shortening cycle (SSC): an active muscle–tendon unit that is stretched immediately before it shortens produces greater work or power than one that shortens alone [9–12].

Although both phenomena are individually well known, they are rarely treated within a single, mechanically explicit model. The kinetic chain is usually described qualitatively, or extracted *a posteriori* from measured kinematics, while the SSC is either invoked verbally or resolved at the level of individual Hill-type muscle–tendon units inside large musculoskeletal frameworks [19, 20]. The former approach does not permit systematic optimization; the latter requires a number of muscle-specific parameters that cannot be constrained from racket-speed data and whose computational cost obscures the underlying physics. For the engineering analysis of racket strokes—equipment studies, timing analysis, and reduced-order simulation—there is a gap between these two extremes: a model in which *release timing* and *active SSC behaviour* are both explicit, low-dimensional, and directly insertable into standard rigid-body simulation.

The present paper is intended to fill that gap. Building on our earlier double- and triple-pendulum studies of energy transfer along the arm–racket chain [6–8], in which the joint torque was a passive restoring torque $\tau_i = -k_i\theta_i$ and release timing emerged implicitly from the coupled dynamics, we make two extensions that together define a unified framework:

1. **Delay as an explicit control parameter.** Each joint can hold its stored elastic energy in a latched state and release it at a freely chosen firing time. The release delay of each joint thereby becomes an explicit, optimizable parameter rather than an emergent by-product of passive dynamics. For two and three active degrees of freedom, a direct scan over the delays locates the firing schedule that maximizes racket-tip speed, and the resulting superadditive speed gain *is* the kinetic chain, quantified.
2. **The SSC as a history-dependent stiffness in the same algorithm.** The shoulder and wrist may additionally pass through an eccentric pre-stretch and active rebound before firing, with the entire SSC represented by an effective torsional stiffness that changes with the motion history. Only two active parameters appear: a rebound gain α and a velocity-dependent firing gain β. Crucially, this SSC block enters the equations of motion through exactly the same joint-torque interface as the delay-programmed springs, so kinetic-chain timing and SSC enhancement are optimized by the same procedure, and their contributions to racket speed can be compared frame by frame within one simulation.

We stress at the outset what the model is and is not. It does not simulate the human musculature; the effective stiffness is a compact joint-level summary of tendon recoil, pre-activation, and reflex contribution, in the same spirit in which effective leg stiffness summarizes elastic behaviour in running and hopping [17, 18]. What the model offers in exchange is analytic transparency—closed-form energy bookkeeping at every active transition—and immediate portability: any planar or spatial rigid-body simulator that accepts a joint torque $\tau(\theta, \dot{\theta})$ can adopt the delay-programmed and SSC blocks without structural modification.

The paper is organized as follows. Section 2 formulates the planar body–arm–racket model. Section 3 analyses the delay-programmed firing model without SSC, progressing from one to three active degrees of freedom and quantifying the kinetic-chain gain. Section 4 introduces the reduced SSC model and its energy bookkeeping, and Section 5 shows that SSC engagement adds speed on top of the delay-optimized kinetic chain within the same firing schedule. Sections 6 and 7 discuss the engineering implications and conclude.

2 Planar three-segment swing model

2.1 Coordinates and segment parameters

The swing is modeled as a planar serial chain composed of three rigid segments: body/trunk, arm, and racket (Fig. 1). The generalized coordinates are

$$\boldsymbol{q} = \begin{bmatrix} \theta_b & \theta_a & \theta_r \end{bmatrix}^T, \tag{1}$$

where θ_b is the absolute body angle, θ_a the arm angle relative to the body, and θ_r the racket angle relative to the arm, so that the absolute arm and racket angles are

$$\phi_a = \theta_b + \theta_a, \qquad \phi_r = \theta_b + \theta_a + \theta_r. \tag{2}$$

The segment parameters used in the simulations are listed in Table 1. Each segment is treated as a uniform slender rod with moment of inertia $I_i = m_i l_i^2/12$ about its own center of mass. The chosen masses and lengths are broadly consistent with reported adult body-segment anthropometry [13], collapsed into a reduced three-segment trunk–arm–racket representation. This reduction sacrifices anatomical detail (e.g., separate upper-arm and forearm segments) in exchange for a model whose dynamics remain analytically transparent, while preserving the inertial contrast between a heavy proximal segment and a light, long distal implement that is central to the physics of interest.

With the base pivot fixed at the origin, the shoulder, wrist, and racket-tip positions are

$$\boldsymbol{p}_1 = l_b \begin{bmatrix} \cos\theta_b \\ \sin\theta_b \end{bmatrix}, \qquad \boldsymbol{p}_2 = \boldsymbol{p}_1 + l_a \begin{bmatrix} \cos\phi_a \\ \sin\phi_a \end{bmatrix}, \qquad \boldsymbol{p}_3 = \boldsymbol{p}_2 + l_r \begin{bmatrix} \cos\phi_r \\ \sin\phi_r \end{bmatrix}, \tag{3}$$

where $\boldsymbol{p}_3$, the racket tip, is taken as the impact point.

Table 1 Segment parameters used in the planar swing model.

Segment	Mass m (kg)	Length l (m)	Moment of inertia I
Body/trunk	25.0	0.50	$m_b l_b^2/12$
Arm	3.0	0.55	$m_a l_a^2/12$
Racket	0.33	0.68	$m_r l_r^2/12$

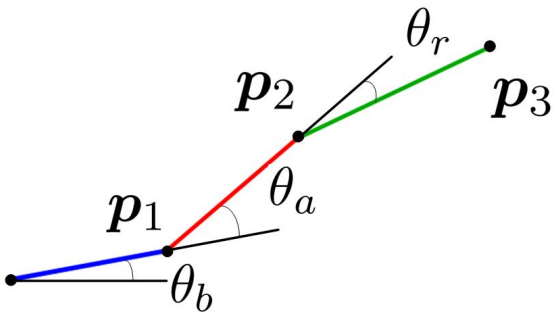


Fig. 1 Planar three-segment body–arm–racket model. The representation is deliberately minimal, but it retains the physical ingredients required to study racket-tip speed: segment inertia, geometric leverage, dynamic (inertial) coupling between segments, and the possibility of a delayed distal release.

2.2 Racket-tip velocity

Differentiating $\boldsymbol{p}_3$ gives the racket-tip velocity components

$$v_x = -l_b\dot{\theta}_b \sin\theta_b - l_a(\dot{\theta}_b + \dot{\theta}_a)\sin\phi_a - l_r(\dot{\theta}_b + \dot{\theta}_a + \dot{\theta}_r)\sin\phi_r, \tag{4}$$

$$v_y = \quad l_b\dot{\theta}_b \cos\theta_b + l_a(\dot{\theta}_b + \dot{\theta}_a)\cos\phi_a + l_r(\dot{\theta}_b + \dot{\theta}_a + \dot{\theta}_r)\cos\phi_r, \tag{5}$$

and the scalar racket-tip speed used throughout as the performance measure is $v_{\mathrm{tip}} = \sqrt{v_x^2 + v_y^2}$.

2.3 Equations of motion

Gravity is neglected because the acceleration phase of interest is short (of order 0.2 s) and the torques generated by the latched springs and by the active joint model of Section 4 dominate the gravitational torque by more than an order of magnitude for the parameters used here. The equations of motion take the standard Lagrangian form for a three-link planar chain,

$$\boldsymbol{M}(\boldsymbol{q})\ddot{\boldsymbol{q}} + \boldsymbol{c}(\boldsymbol{q}, \dot{\boldsymbol{q}}) = \boldsymbol{\tau}, \tag{6}$$

where $\boldsymbol{M}(\boldsymbol{q})$ is the configuration-dependent mass matrix and $\boldsymbol{c}(\boldsymbol{q}, \dot{\boldsymbol{q}})$ collects the Coriolis and centrifugal terms; the explicit entries are given in Appendix A. The single

point of contact between the biomechanics and the rigid-body dynamics is the joint torque vector $\boldsymbol{\tau}$, supplied either by the delay-programmed latched springs of Section 3 or by the SSC-augmented torques of Section 4. It is this clean interface that makes both mechanisms directly transferable to any general-purpose simulation environment. Equation (6) is integrated numerically (fourth-order Runge–Kutta, fixed step) for all results reported below; the only place an analytic solution is used, as a consistency check, is the single-active-joint case of Section 3.2.

3 Delay-programmed firing without SSC

3.1 Elastic energy and latch angles

The baseline firing model uses constant torsional spring constants

$$k_b = 300\,\mathrm{N\,m\,rad^{-1}}, \qquad k_a = 100\,\mathrm{N\,m\,rad^{-1}}, \qquad k_r = 10\,\mathrm{N\,m\,rad^{-1}}. \tag{7}$$

These values are not fitted to dynamometric measurements from a specific athlete; following the strategy of our earlier pendulum studies [6, 7], they are chosen to reproduce, at an order-of-magnitude level, the well-documented proximal-to-distal decrease in maximal joint-torque capacity: the trunk/hip complex sustains the largest restoring torque, the shoulder an intermediate torque, and the wrist the smallest. This ordering, $k_b > k_a > k_r$, is qualitatively consistent with segmental descriptions of proximal-to-distal torque and timing in throwing and striking motions [1, 2, 4] and with simple optimal-timing analyses of muscle activation in throwing-like tasks [14]. The qualitative conclusions drawn below—the ranking of single-joint speeds, the existence of an optimal release delay, and the superadditive character of multi-joint release—depend on this ordering and on the associated inertial hierarchy of the segments, not on the third significant figure of k_i.

The target equilibrium posture is

$$\theta_b^{\mathrm{eq}} = 0^\circ, \qquad \theta_a^{\mathrm{eq}} = 30^\circ, \qquad \theta_r^{\mathrm{eq}} = -30^\circ, \tag{8}$$

so that the absolute racket angle at the target is approximately horizontal, $\phi_r^{\mathrm{eq}} = 0^\circ$. This configuration is representative of the extended-arm, slightly laid-back-wrist posture reported at, or immediately before, ball contact in the tennis serve and forehand drive [3, 15]. Its role in the model is not merely descriptive: v_{tip} is evaluated as each active joint angle $\theta_i(t)$ passes through θ_i^{eq}, and the firing-time optimization of Sections 3.3–3.4 is a search for the set of release delays that brings every active joint through its own θ_i^{eq} with maximum angular velocity at essentially the same instant—the same frame. This construction is the model-level analogue of the moment of maximal segment extension used to characterize efficient timing in our earlier pendulum-based descriptions of the kinetic chain [6, 7].

The initial latched posture is

$$\theta_b^0 = -45^\circ, \qquad \theta_a^0 = -30^\circ, \qquad \theta_r^0 = -100^\circ, \tag{9}$$

representing an exaggerated, maximally "cocked" backswing: the trunk counter-rotated away from the target, the upper arm drawn behind the trunk, and the racket laid back sharply relative to the forearm. Postures of this general character are the mechanical prerequisite for proximal-to-distal energy transfer documented in high-speed serves and ground strokes [2–4]. Within the model, θ_i^0 is the configuration at which elastic energy is stored, in direct analogy with the eccentric pre-loading that precedes the concentric phase of a genuine SSC [14]; Section 4 makes this analogy explicit for the shoulder and wrist.

The stored elastic energy at joint i is

$$E_i = \tfrac{1}{2} k_i (\theta_i^{\mathrm{eq}} - \theta_i^0)^2, \tag{10}$$

giving

$$E_b = 92.53\,\mathrm{J}, \quad E_a = 54.83\,\mathrm{J}, \quad E_r = 7.46\,\mathrm{J}, \quad E_{\mathrm{total}} \simeq 154.82\,\mathrm{J}. \tag{11}$$

The essential modeling assumption is that each joint can be latched and released at an independently chosen time. Once released, joint i produces the restoring torque

$$\tau_i = k_i (\theta_i^{\mathrm{eq}} - \theta_i); \tag{12}$$

prior to release it remains held at θ_i^0, and if it is inactive in a reduced-degree-of-freedom simulation it is held at θ_i^{eq}. This construction deliberately separates two quantities that are inseparable in an unconstrained passive pendulum: (i) the amount of elastic energy available at each joint, fixed once θ_i^0, θ_i^{eq}, and k_i are specified, and (ii) the instant at which that energy is released, left as a free parameter—the firing time, or equivalently the release delay relative to the other joints. Because v_{tip} depends sensitively on the relative firing times once more than one joint is active, this separation is what allows the release delay to be optimized directly, rather than emerging implicitly from the passive coupled dynamics as in our earlier pendulum models [6, 7].

3.2 One active degree of freedom

When only joint j is active, the remaining joints are held fixed at θ^{eq} and the multi-body dynamics reduce, at the instant θ_j crosses θ_j^{eq}, to a single scalar energy balance,

$$\tfrac{1}{2} k_j (\theta_j^{\mathrm{eq}} - \theta_j^0)^2 = \tfrac{1}{2} M_{jj}^* \omega_j^2, \tag{13}$$

where M_{jj}^* is the effective scalar inertia of coordinate j evaluated at θ^{eq}. Hence

$$\omega_j = \sqrt{2E_j / M_{jj}^*}, \tag{14}$$

and substitution into Eqs. (4)–(5) gives a closed-form prediction for v_{tip} that can be compared directly with the numerically integrated trajectory (Table 2).

The shoulder-only case yields the highest single-joint speed. The shoulder spring stores substantial energy and acts through the long arm-plus-racket lever; the wrist has small effective inertia and can spin up rapidly, but its stored energy is limited by

Table 2 Single-active-joint (1-DOF) results. The closed-form energy-conversion estimate and the peak speed obtained from numerical integration of Eq. (6) agree to the precision shown, confirming the internal consistency of the numerical model.

Active joint	Initial condition	Analytic v_{tip} (m/s)	Simulated $v_{\max}$ (m/s)
Body only	$\theta_b^0 = -45^\circ$	10.815	10.815
Shoulder only	$\theta_a^0 = -30^\circ$	16.631	16.631
Wrist only	$\theta_r^0 = -100^\circ$	11.649	11.649

the small torque constant k_r; and the trunk, although it stores the largest energy of the three, rotates the entire chain rigidly about the base pivot rather than producing distal angular magnification, so much of its stored energy is converted into motion of the proximal mass rather than into racket-tip speed. No single joint, however, approaches the speeds reported for high-level strokes; the remaining sections show that the missing ingredient is timing, not stored energy.

3.3 Two active degrees of freedom

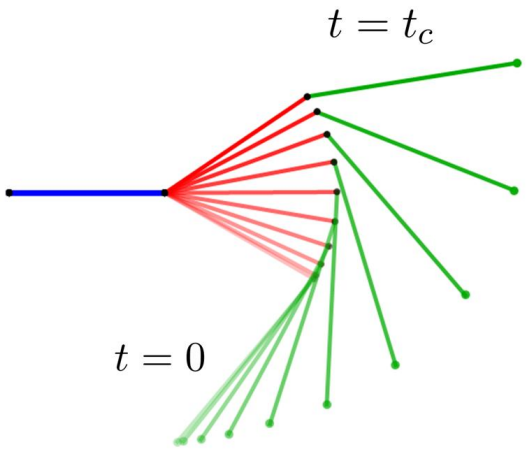


Fig. 2 Two-degree-of-freedom (shoulder+wrist) release at the optimal delay $\Delta t = 0.040\,\mathrm{s}$ of Table 3, with the trunk held fixed at θ_b^{eq} throughout. Ten superimposed configurations of the arm–racket linkage are shown at equal time intervals from $t = 0$ (lightest, lower trace) to the impact time $t = t_c$ (darkest, upper trace). The shoulder joint releases its stored elastic energy at $t = 0$; the wrist joint releases its own stored energy 0.04 s later. This lag allows the racket to begin accelerating only after the shoulder has already imparted substantial angular velocity to the arm, so that the racket tip attains its maximum speed close to $t = t_c$ rather than earlier in the motion.

With two active joints, the distal joint is released a time Δt after the proximal joint. Once two joints move simultaneously, the dynamics are no longer reducible to a single scalar energy balance, because the mass matrix $\boldsymbol{M}(\boldsymbol{q})$ depends on configuration and kinetic energy is continuously exchanged between coordinates through the off-diagonal terms h_{12}, h_{13}, h_{23} (Appendix A). The qualitative mechanism, illustrated in Fig. 2, is nevertheless straightforward: the proximal joint first accelerates the larger, slower segment, and the distal joint is then released into an already-moving mechanical environment. If the distal release occurs too early, the distal segment accelerates before the proximal segment has built up appreciable momentum, and the coupling benefit is lost; if it occurs too late, the distal segment reaches its own θ^{eq} after the optimal hitting configuration has already been passed. An optimal, interior value of Δt therefore exists for every joint pair, and was located here by a one-dimensional numerical scan of $v_{\mathrm{tip}}(\Delta t)$ at the impact time (Table 3).

Table 3 Optimized 2-DOF results. For each joint pair, the release delay Δt of the distal joint relative to the proximal joint was scanned numerically, and the delay that maximizes v_{tip} at impact is reported together with the corresponding maximum speed.

Active joints	Optimal delay (s)	Maximum v_{tip} (m/s)
Body + shoulder	0.160	25.758
Body + wrist	0.107	23.948
Shoulder + wrist	0.040	30.156

The shoulder–wrist pair produces the largest two-joint speed. The shoulder supplies a strong mid-chain acceleration over a comparatively large angular excursion, while the wrist, owing to its small effective inertia and long distal lever arm, converts a comparatively modest angular velocity into a rapid final "snap" of the racket, as visible in the final traces of Fig. 2.

3.4 Three active degrees of freedom

With all three joints active, the trunk is fired at $t = 0$ while the shoulder and wrist firing times, t_{shoulder} and t_{wrist}, are treated as two independent free parameters. Because the three-joint dynamics couple through the full mass matrix $\boldsymbol{M}(\boldsymbol{q})$, no closed-form expression analogous to Section 3.2 is available; the optimal pair $(t_{\mathrm{shoulder}}, t_{\mathrm{wrist}})$ was instead located by a two-dimensional numerical search that maximizes v_{tip} at the impact time t_c. The resulting optimum is

$$t_{\mathrm{shoulder}} = 0.149\,\mathrm{s}, \qquad t_{\mathrm{wrist}} = 0.195\,\mathrm{s}, \tag{15}$$

giving

$$v_{\mathrm{tip,max}} = 43.122\,\mathrm{m\,s^{-1}}, \tag{16}$$

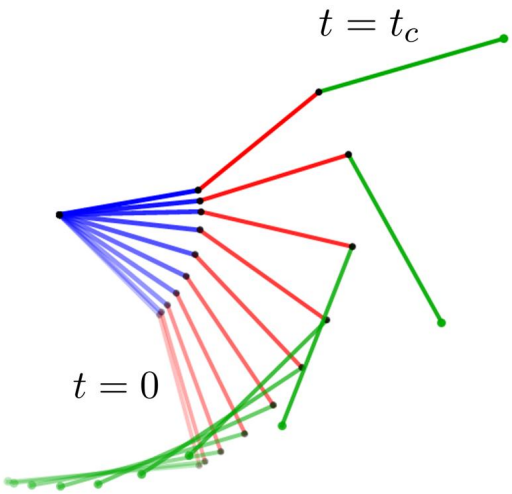


Fig. 3 Fully optimized three-degree-of-freedom (body+shoulder+wrist) release. Using the same convention as Fig. 2, ten superimposed configurations of the complete body–arm–racket chain are shown at equal time intervals from $t = 0$ (lightest, lower trace) to the impact time $t = t_c$ (darkest, upper trace). The trunk rotates throughout the entire interval from $t = 0$; the arm begins rotating relative to the trunk only after the shoulder release delay $t_{\text{shoulder}} = 0.149\,\text{s}$; and the racket begins rotating relative to the arm only after the wrist release delay $t_{\text{wrist}} = 0.195\,\text{s}$, i.e., $0.046\,\text{s}$ after the shoulder. As a result, the racket orientation changes little during the early part of the motion and then sweeps through a large angle in the final fraction of the swing, producing the clearly visible whip-like acceleration that yields the maximum tip speed essentially at $t = t_c$.

a value that falls within the range reported for high-level tennis strokes and serves [3, 5, 15]. More significant than the absolute value is that the optimization has discovered, purely numerically, a firing schedule in which the trunk begins moving first, the shoulder is released only after the trunk has accumulated angular momentum, and the wrist/racket is released last, once the arm itself is moving rapidly—precisely the proximal-to-distal sequence associated with the kinetic chain. At the optimum, all three joints pass through their equilibrium angles with maximal angular velocity at essentially the same frame; when the delays are tuned in this way, effectively all of the recoverable stored energy is channelled into racket motion at impact.

Each optimal delay found here plays the same physical role as the sequential release timing analyzed in our earlier triple-pendulum study, where allowing the relative timing of segment release to be controlled explicitly was shown to increase the distal-segment speed beyond what a purely passive kinetic-chain release could achieve [7]. The delay-optimization procedure used here is the active-control counterpart of that mechanism: energy stored during the backswing is not allowed simply to propagate outward according to the natural (passive) dynamics of the coupled links, but

is deliberately released joint by joint at the instant that best exploits the growing angular velocity of the more proximal segments.

Figure 4 collects all of the non-SSC firing results. The progression from the best single-joint case ($16.63\,\mathrm{m\,s^{-1}}$, shoulder) to the best two-joint case ($30.15\,\mathrm{m\,s^{-1}}$, shoulder+wrist) to the three-joint case ($43.12\,\mathrm{m\,s^{-1}}$) is markedly superadditive: the three-joint speed exceeds twice the best single-joint speed, even though only one further degree of freedom (the trunk) was added relative to the best two-joint case. This nonlinear scaling is the numerical signature of the kinetic chain: each additional proximal segment, when correctly timed, does not simply contribute its own share of racket speed but multiplies the effectiveness of the more distal segments by delivering them into motion with a higher base angular velocity before they, in turn, fire.

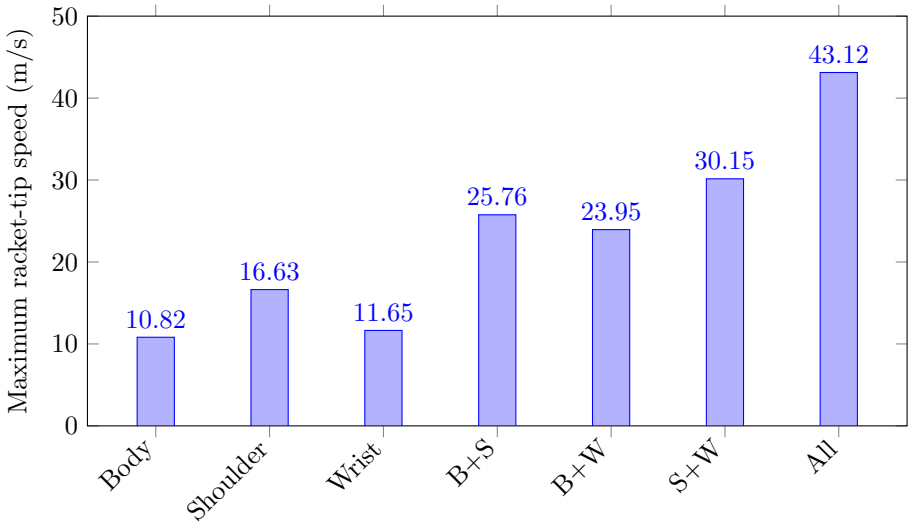


Fig. 4 Maximum racket-tip speed for every non-SSC firing configuration studied in Section 3. Increasing the number of correctly delayed active degrees of freedom increases racket speed superadditively; the largest speed is reached only when trunk, shoulder, and wrist fire sequentially with the optimized delays of Section 3.4.

4 Reduced active stretch–shortening-cycle model

4.1 Physiological motivation and modeling principle

Section 3 treated each joint as a passive spring released at a programmed time. A biological joint, however, is not a spring of fixed stiffness. The SSC refers to the enhancement of force, power, or work output that occurs when an active muscle–tendon unit is stretched immediately before it shortens [9–11]. This enhancement is not attributable to a single cause but to several mechanisms acting in concert: elastic energy storage and recoil in tendon and aponeurosis; a higher force at the onset of shortening due to pre-activation; force enhancement associated with the eccentric

loading history; and a neural reflex contribution when the imposed stretch is rapid. That these mechanisms act jointly, at a scale relevant to whole-limb performance, is demonstrated by the classical finding that a countermovement jump outperforms a concentric-only squat jump [16].

It is precisely this whole-limb, joint-torque level of description that is relevant here. A physiologically complete SSC model would require many muscle-specific parameters that cannot be constrained from racket-speed data; we therefore adopt the reduced joint-level description

$$\tau_i \simeq k_{i,\mathrm{eff}}\big(t, \theta_i, \dot{\theta}_i, \mathrm{history}\big)\big(\theta_i^{\mathrm{eq}} - \theta_i\big), \tag{17}$$

in which $k_{i,\mathrm{eff}}$ is emphatically not a passive material constant but an effective, history-dependent stiffness summarizing the net contribution of tendon recoil, pre-activation, and reflex action to the joint torque. Because Eq. (17) has the same interface as the passive springs of Section 3—a torque as a function of joint state—the SSC block slots into the delay-programmed framework, and into any general rigid-body simulation, without structural modification. The kinetic-chain optimization and the SSC enhancement are thereby handled by one and the same algorithm.

4.2 Torque phases of the active joint model

We describe the shoulder and wrist torque $\tau(\theta, \dot{\theta})$ as passing through four physically motivated phases: *free*, *pre-stretch*, *active rebound*, and *main firing* (Fig. 5). Each phase is defined by an explicit torque expression, so that the point at which mechanical energy is injected beyond what a purely passive spring would supply is stated unambiguously.

Before the joint angle reaches the latch region, no elastic torque acts,

$$\tau_{\mathrm{free}} = 0, \tag{18}$$

corresponding to the unloaded part of the preparatory motion, prior to engagement of the muscle–tendon unit against its series-elastic limit.

Once θ moves past the latch angle θ_L into the stretched region, a stiff bump spring resists further stretch,

$$\tau_{\mathrm{stretch}}(\theta) = -k_{\mathrm{bump}}(\theta - \theta_L), \tag{19}$$

representing the combined passive loading of tendon and connective tissue and an initial level of active muscle tension during the eccentric phase, i.e., while the joint is being decelerated at the end of the backswing.

The transition to the genuinely active part of the model occurs at the instant the angular velocity reverses sign—the moment the joint begins to shorten. At that instant the effective stiffness of the bump spring is increased by a factor $(1 + \alpha)$,

$$\tau_{\mathrm{rebound}}(\theta) = -(1 + \alpha)\, k_{\mathrm{bump}}(\theta - \theta_L), \tag{20}$$

which is the explicit representation, within this reduced model, of the pre-activation and short-range stiffness enhancement documented to accompany the stretch-to-shortening transition [9–11]. This is the step that distinguishes the present model from a purely passive spring: the effective stiffness itself changes as a function of the motion history—specifically, of the sign reversal of $\dot{\theta}$—rather than remaining constant throughout the motion.

Finally, once θ crosses back over the latch angle, the main joint spring fires toward the target equilibrium angle with a velocity-dependent gain,

$$\tau_{\text{fire}}(\theta) = k\, f(\omega_{\text{in}})\,(\theta^{\text{eq}} - \theta), \qquad f(\omega_{\text{in}}) = 1 + \min\big(g_{\max}, \beta|\omega_{\text{in}}|\big), \tag{21}$$

where ω_{in} is the angular velocity of the joint at the instant it first entered the stretched region and $g_{\max}$ caps the maximum stiffness enhancement.

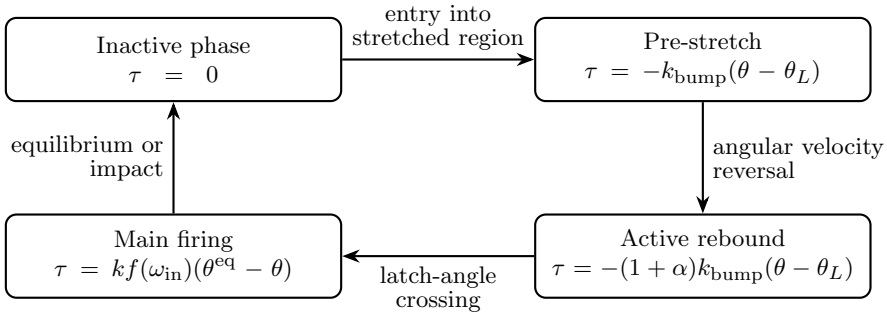


Fig. 5 Event-based effective-torque sequence used in the reduced SSC model. The diagram does not represent four independent physical springs; it indicates how the effective joint torque changes as the joint enters the pre-stretch region, reverses its angular velocity, and proceeds to the main firing phase. Because each phase is a torque law of the joint state alone, the entire sequence can be inserted into any rigid-body simulator through the same interface as a passive spring.

The sequence $\tau_{\text{free}} \to \tau_{\text{stretch}} \to \tau_{\text{rebound}} \to \tau_{\text{fire}}$ constitutes the complete active-joint model used for the shoulder and wrist. Beyond the passive spring constants of Section 3, it requires only k_{bump}, θ_L, and the two active parameters α and β (with the saturation $g_{\max}$), yet it reproduces the qualitative signature of a genuine SSC: passive loading during the stretch, an abrupt active stiffening at the moment of reversal, and an enhanced, velocity-dependent release. The parameter values used in all SSC simulations are listed in Table 4. The bump stiffness is taken as five times the baseline stiffness of each joint, and the reference angular velocities ω_{ref} reflect the characteristic pre-stretch rates of the shoulder and wrist, so that $\beta = g_{\max}/\omega_{\text{ref}}$ maps a typical eccentric entry velocity onto the maximum 10% firing gain.

4.3 Energy input by stiffness modulation

The active-joint model injects mechanical energy at two identifiable events, which can be quantified exactly. Let $\delta = \theta - \theta_L$ denote the compression of the bump spring.

Table 4 Parameters used in the reduced SSC model.

Parameter	Shoulder	Wrist
Baseline stiffness k ($\mathrm{N\,m\,rad^{-1}}$)	100	10
Bump factor	5.0	5.0
k_{bump} ($\mathrm{N\,m\,rad^{-1}}$)	500	50
Active bump gain α	0.10	0.10
Maximum firing gain $g_{\max}$	0.10	0.10
Reference angular velocity ω_{ref} ($\mathrm{rad\,s^{-1}}$)	20	80
$\beta = g_{\max}/\omega_{\mathrm{ref}}$ ($\mathrm{s\,rad^{-1}}$)	0.0050	0.00125

When the effective stiffness changes from k_{bump} to $(1+\alpha)k_{\mathrm{bump}}$ at constant δ, the instantaneously stored potential energy increases by

$$\Delta E_{\mathrm{rebound}} = \tfrac{1}{2}\alpha k_{\mathrm{bump}}\delta^2, \tag{22}$$

which we interpret as active metabolic input expressed through an increase in joint stiffness rather than through an explicit force term. Similarly, when the main spring fires with gain $f(\omega_{\mathrm{in}}) > 1$, the elastic energy available to accelerate the joint toward θ^{eq} increases by

$$\Delta E_{\mathrm{fire}} = \tfrac{1}{2}k\big[f(\omega_{\mathrm{in}}) - 1\big](\theta^{\mathrm{eq}} - \theta)^2. \tag{23}$$

The model therefore admits explicit energy bookkeeping: between the two active transitions the mechanical system evolves conservatively under Eq. (6), while at each transition a well-defined quantity of active energy, $\Delta E_{\mathrm{rebound}}$ or ΔE_{fire}, is injected into the joint. This bookkeeping is what allows the SSC contribution to racket speed to be isolated cleanly from the kinetic-chain contribution in the combined simulations of Section 5.

4.4 Why effective stiffness is a useful SSC variable

Representing SSC action through a variable effective stiffness offers four practical advantages. First, it enters the rigid-body equations of motion directly through the joint torque, requiring no additional state beyond $(\theta, \dot{\theta})$ and a small number of history flags; any simulation built on Eq. (6)—or on its spatial generalization—can adopt it as a drop-in replacement for a passive joint spring. Second, being low-dimensional, it is in principle identifiable from joint-level motion data far more readily than a multi-muscle Hill-type model, in the same spirit in which an effective leg or joint stiffness has long been used to characterize elastic behaviour in running and hopping [17, 18]. Third, it naturally reproduces the empirical observation that a stronger or faster pre-stretch increases the power available during the subsequent shortening phase. Fourth, it predicts that different athletes should require different optimal preparatory postures: a player with large α and β stands to gain more from a pronounced pre-stretch, whereas a player with small α and β may be better served by a posture optimized primarily for passive elastic release.

5 SSC-enhanced simulation results

The combined simulations use the fully optimized three-joint firing schedule of Section 3.4 unchanged, with the shoulder and wrist joints now governed by the four-phase torque sequence of Section 4.2 and the parameters of Table 4. The four cases in Table 5 differ only in the imposed initial shoulder and wrist angular velocities at $t = 0$; a negative velocity corresponds to the arm or racket still moving backward, i.e., an imposed pre-stretch or additional backswing loading, at the reference instant.

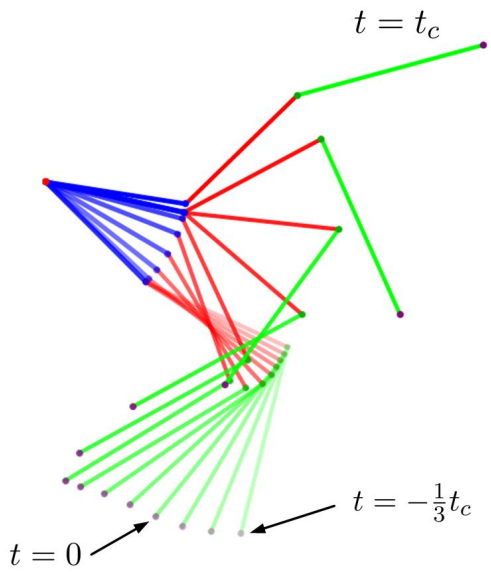


Fig. 6 SSC-enhanced swing with both shoulder and wrist pre-stretched, $(\dot{\theta}_a(0), \dot{\theta}_r(0)) = (-2, -4)$ rad/s, and initial angles $\theta_a = 12.0°$, $\theta_r = -96.0°$ at $t = 0$. In contrast to Figs. 2 and 3, the configurations shown here begin *before* the reference instant, at $t = -t_c/3$, so as to display explicitly the backswing portion of the motion during which the arm and racket are still moving backward under the imposed pre-stretch condition. The sequence then proceeds through $t = 0$ and on to the impact time $t = t_c$, again with ten configurations shown at equal time intervals. The initial convergence and subsequent reversal of the early, light-colored traces is the kinematic signature of the pre-stretch phase of the SSC (τ_{stretch} in Section 4.2), which precedes the active rebound and main firing that ultimately accelerate the racket.

Three features of Table 5 deserve emphasis. First, relative to the non-SSC optimized three-joint result, $v_{\text{tip,max}} = 43.12\,\text{m}\,\text{s}^{-1}$, the SSC model with both joints pre-stretched reaches $v_{\text{tip,max}} = 46.74\,\text{m}\,\text{s}^{-1}$, a relative enhancement of

$$\frac{46.74 - 43.12}{43.12} \times 100\% \simeq 8.4\%. \tag{24}$$

Second, and central to the unified-framework argument of this paper, the impact time shifts by no more than 3 ms across all four cases: the SSC adds speed *within*

Table 5 Representative SSC-enhanced results. All cases use the same firing schedule as the optimized non-SSC 3-DOF case of Section 3.4; only the imposed initial shoulder and wrist angular velocities differ.

Case	$(\dot{\theta}_a(0), \dot{\theta}_r(0))$ (rad/s)	Peak speed (m/s)	Impact time (s)
No imposed pre-stretch	$(0, 0)$	42.95	0.218
Shoulder pre-stretch	$(-2, 0)$	43.52	0.218
Wrist pre-stretch	$(0, -4)$	46.30	0.220
Both pre-stretched	$(-2, -4)$	46.74	0.221

the delay-optimized firing schedule, so that the maximum racket speed is attained at essentially the same frame at which the kinetic-chain optimization alone would place it. Active stiffness modulation and delay programming are therefore not competing mechanisms requiring separate tuning; the same scan that optimizes the kinetic chain accommodates the SSC contribution without re-optimization. Third, the wrist pre-stretch contributes more than the shoulder pre-stretch for the parameter set used here. This asymmetry is expected on physical grounds: the wrist acts closest to the racket and has the smallest effective inertia among the three joints, so a modest active stiffness increase at the wrist is amplified, through the same lever effect responsible for the single-joint ranking of Table 2, into a comparatively large distal angular velocity.

The 8.4% figure should not be read as a universal constant of tennis biomechanics. Within the model, α and β stand in for an individual athlete's capacity to exploit the SSC; the values in Table 4 are chosen for illustration rather than fitted to a specific player. Because the resulting enhancement of v_{tip} scales with α and β, an athlete with greater eccentric strength, tendon stiffness, or reflex contribution would be expected to realize a correspondingly larger enhancement, and vice versa. The essential conclusion is the qualitative, mechanistic result that active, history-dependent joint stiffening adds speed on top of the delay-optimized kinetic-chain value, by an amount that is inherently athlete-specific.

This athlete-specific character is also visible in the geometry of the motion itself. Comparing the SSC-enhanced swing of Fig. 6 with the purely passive, optimized three-joint swing of Fig. 3 reveals a noticeably different body–arm–racket trajectory, even though both simulations are optimized, in their respective senses, for maximum racket-tip speed. Different combinations of α, β, and pre-stretch velocity in general produce different optimal postures and visibly different swing shapes, each of which can nonetheless achieve close to maximal racket-tip speed for the corresponding parameter set. For a high-speed stroke this enhancement is mechanically meaningful: because outgoing ball speed depends strongly on racket speed at impact, even an 8–9% increase in racket-tip speed can translate into a practically significant difference in shot performance.

6 Discussion

The central methodological claim of this paper is that two mechanisms usually treated at very different levels of description—the kinetic chain, ordinarily discussed kinematically, and the SSC, ordinarily discussed at the muscle–tendon level—can be captured within one joint-torque algorithm that is simple enough to insert into any standard rigid-body simulation. The results of Sections 3 and 5 support this claim in two steps.

The delay-programmed model of Section 3 establishes the kinetic-chain result quantitatively: racket-tip speed increases from about $16.6\,\mathrm{m\,s^{-1}}$ for the best single active joint, to $30.2\,\mathrm{m\,s^{-1}}$ for the best pair, to $43.1\,\mathrm{m\,s^{-1}}$ once trunk, shoulder, and wrist are all released with optimized delays. This progression is not a numerical artifact of the optimization procedure; it follows directly from the inertial coupling encoded in the off-diagonal terms of $\boldsymbol{M}(\boldsymbol{q})$, the geometric leverage provided by the increasing distance of each successive segment from the base pivot, and the existence of a well-defined optimal release delay for each joint pair, as demonstrated analytically for the single-joint case and numerically for two and three joints. When the two (2-DOF) or three (3-DOF) delays are tuned to their optima, every joint passes through its equilibrium angle with maximal angular velocity at essentially the same frame, and the stored energy is channelled almost entirely into racket motion at impact.

The SSC model of Section 4 then adds a physiologically motivated mechanism—active, history-dependent energy input at the joint—without changing the algorithmic structure. Because the SSC enters as a torque law of the joint state, the same firing schedule, the same integration scheme, and the same speed-at-impact objective apply unchanged, and the representative simulations of Section 5 show that SSC engagement raises the peak speed by roughly 8% at essentially the same impact frame. In other words, delay programming determines *when* energy arrives at the racket, and the SSC parameters (α, β) determine *how much additional* energy is injected en route; the two are composable rather than conflicting.

Several implications extend beyond the specific numbers reported here. Foremost, efficient racket acceleration is a problem of *timing* as much as of strength: a wrist fired too early cannot reach maximal speed because it fails to exploit the angular momentum already generated by the more proximal segments, whereas a correctly delayed release allows the racket to accelerate only once the trunk and arm have already been set in motion. Second, the SSC results indicate that the preparatory phase of the stroke—racket lag, shoulder loading, and the rapid reversal from backswing to forward swing—is not merely a stylistic feature of elite technique but a mechanism that can genuinely increase the joint torque available during the forward swing. Third, the optimal posture, timing, and even the outward shape of the swing should be expected to differ from one athlete to another: players with different α, β, and characteristic pre-stretch velocity are predicted to reach their own maximum racket speed through visibly different combinations of posture and timing, as illustrated by the marked difference between Figs. 3 and 6. This observation motivates a note of caution for coaching practice: because the swing shapes observed in professional footage reflect that athlete's own α, β, and strength characteristics, the model raises the hypothesis—though it does not by itself constitute proof—that an amateur who reproduces only the outward form of a professional stroke, without comparable underlying SSC capacity, is

not guaranteed the same racket-speed benefit. Fourth, because segment mass, length, joint stiffness, release timing, and SSC gain all appear as separate, explicit parameters, the model can be used to explore how changes in racket mass, arm length, or an athlete's strength profile shift the optimal firing schedule—a feature of direct interest for equipment selection and racket–player matching in sports engineering.

These implications should be read in light of the model's deliberate simplifications. The model is planar and excludes shoulder internal/external rotation, forearm pronation–supination, grip and string-bed compliance, aerodynamic drag, and the finite-duration ball–racket collision process. The arm is a single rigid segment, and the SSC description is phenomenological, formulated at the level of net joint torque rather than resolved into individual muscle–tendon units as in full musculoskeletal frameworks [19, 20]. The specific numerical values reported (parameter choices, optimal delays, enhancement percentages) should accordingly be regarded as illustrative of the underlying mechanisms rather than as normative targets. We regard this simplicity, however, as the model's principal virtue: by isolating a small number of physically distinct mechanisms—elastic storage, delayed release, inertial coupling, distal whip-like amplification, and active history-dependent energy input—the model renders the logic of efficient racket acceleration transparent in a way that is difficult to extract from a high-dimensional musculoskeletal simulation, while remaining explicit enough that each mechanism can be switched on or off, or its parameters varied, to test a specific hypothesis.

7 Conclusions

We have developed a minimal planar body–arm–racket model of the tennis swing in which release timing and stretch–shortening-cycle enhancement are handled by a single joint-torque algorithm. Separating stored elastic energy from release timing converts the delay between successive joint releases into an explicit, optimizable parameter; for one active joint the closed-form energy-conversion estimate matches the numerically integrated racket-tip speed exactly, validating the numerical procedure. Optimizing the delays for two and three active joints produces a distinctly superadditive increase in racket-tip speed—from $16.6\,\mathrm{m\,s^{-1}}$ to $30.2\,\mathrm{m\,s^{-1}}$ to $43.1\,\mathrm{m\,s^{-1}}$—with all joints passing through their equilibrium angles at essentially the same frame, which is the quantitative content of the kinetic-chain principle. Adding the reduced SSC model, in which the effective stiffness of the shoulder and wrist increases through a pre-stretch and rebound phase before firing with a velocity-dependent gain governed by only two active parameters (α, β), raises the peak speed to $46.7\,\mathrm{m\,s^{-1}}$ ($\approx 8\%$) within the same firing schedule and at the same impact frame. Because the SSC block shares the torque interface of the passive springs, both mechanisms can be inserted directly into general rigid-body simulations of racket strokes, and their contributions compared frame by frame. While the model does not simulate the human musculature, it provides an analytically transparent, computationally inexpensive framework for studying racket sports as simple physical systems—and, because the enhancement and the optimal preparatory posture scale with the athlete-specific parameters α and β, it indicates that efficient technique

is inherently individual, with direct implications for personalized swing optimization, training design, and racket–player matching.

Acknowledgments. The author thanks colleagues for helpful discussions.

Declarations

Conflict of interest. The author declares no conflict of interest.

Data availability. The simulation code and data supporting the findings of this study are available from the corresponding author on reasonable request.

Appendix A Mass matrix and Coriolis terms

Writing $c_a = \cos\theta_a$, $c_r = \cos\theta_r$, $c_{ar} = \cos(\theta_a + \theta_r)$, the symmetric mass matrix in Eq. (6) is

$$\boldsymbol{M} = \begin{bmatrix} h_{11} & h_{12} & h_{13} \\ h_{12} & h_{22} & h_{23} \\ h_{13} & h_{23} & h_{33} \end{bmatrix}, \tag{A1}$$

with entries

$$\begin{aligned} h_{11} &= I_b + m_b\Big(\tfrac{l_b}{2}\Big)^2 + I_a + m_a\Big(l_b^2 + \Big(\tfrac{l_a}{2}\Big)^2 + l_b l_a c_a\Big) \\ &\quad + I_r + m_r\Big(l_b^2 + l_a^2 + \Big(\tfrac{l_r}{2}\Big)^2 + 2l_b l_a c_a + l_b l_r c_{ar} + l_a l_r c_r\Big), \end{aligned} \tag{A2}$$

$$\begin{aligned} h_{12} &= I_a + m_a\Big(\Big(\tfrac{l_a}{2}\Big)^2 + \tfrac{1}{2} l_b l_a c_a\Big) + I_r \\ &\quad + m_r\Big(l_a^2 + \Big(\tfrac{l_r}{2}\Big)^2 + l_b l_a c_a + \tfrac{1}{2} l_b l_r c_{ar} + l_a l_r c_r\Big), \end{aligned} \tag{A3}$$

$$h_{13} = I_r + m_r\Big(\Big(\tfrac{l_r}{2}\Big)^2 + \tfrac{1}{2} l_a l_r c_r + \tfrac{1}{2} l_b l_r c_{ar}\Big), \tag{A4}$$

$$h_{22} = I_a + m_a\Big(\tfrac{l_a}{2}\Big)^2 + I_r + m_r\Big(l_a^2 + \Big(\tfrac{l_r}{2}\Big)^2 + l_a l_r c_r\Big), \tag{A5}$$

$$h_{23} = I_r + m_r\Big(\Big(\tfrac{l_r}{2}\Big)^2 + \tfrac{1}{2} l_a l_r c_r\Big), \tag{A6}$$

$$h_{33} = I_r + m_r\Big(\tfrac{l_r}{2}\Big)^2. \tag{A7}$$

The Coriolis/centrifugal vector follows from the usual Christoffel-symbol construction,

$$c_i = \sum_{j=1}^{3}\sum_{k=1}^{3} \frac{1}{2}\left(\frac{\partial M_{ij}}{\partial q_k} + \frac{\partial M_{ik}}{\partial q_j} - \frac{\partial M_{jk}}{\partial q_i}\right)\dot{q}_j \dot{q}_k. \tag{A8}$$

References

[1] Putnam CA (1993) Sequential motions of body segments in striking and throwing skills: descriptions and explanations. J Biomech 26(Suppl 1):125–135. https://doi.org/10.1016/0021-9290(93)90084-R

[2] Sprigings E, Marshall R, Elliott B, Jennings L (1994) A three-dimensional kinematic method for determining the effectiveness of arm segment rotations in producing racquet-head speed. J Biomech 27(3):245–254. https://doi.org/10.1016/0021-9290(94)90001-9

[3] Elliott B, Marshall R, Noffal G (1995) Contributions of upper limb segment rotations during the power serve in tennis. J Appl Biomech 11(4):433–442. https://doi.org/10.1123/jab.11.4.433

[4] Marshall RN, Elliott BC (2000) Long-axis rotation: the missing link in proximal-to-distal segmental sequencing. J Sports Sci 18(4):247–254. https://doi.org/10.1080/026404100364983

[5] Elliott B (2006) Biomechanics and tennis. Br J Sports Med 40(5):392–396. https://doi.org/10.1136/bjsm.2005.023150

[6] Youn S-H (2015) Double pendulum model for a tennis stroke including a collision process. J Korean Phys Soc 67(7):1110–1117. https://doi.org/10.3938/jkps.67.1110

[7] Youn S-H (2017) Going beyond the kinetic chain process in a swing by using a triple pendulum model. J Korean Phys Soc 70(7):656–665. https://doi.org/10.3938/jkps.70.656

[8] Youn S-H (2023) Push vs. hit, the most efficient stroke in the kinetic chain process. J Korean Phys Soc 82(7):629–637. https://doi.org/10.1007/s40042-023-00751-8

[9] Cavagna GA, Dusman B, Margaria R (1968) Positive work done by a previously stretched muscle. J Appl Physiol 24(1):21–32. https://doi.org/10.1152/jappl.1968.24.1.21

[10] Komi PV (2000) Stretch-shortening cycle: a powerful model to study normal and fatigued muscle. J Biomech 33(10):1197–1206. https://doi.org/10.1016/S0021-9290(00)00064-6

[11] Nicol C, Avela J, Komi PV (2006) The stretch-shortening cycle: a model to study naturally occurring neuromuscular fatigue. Sports Med 36(11):977–999. https://doi.org/10.2165/00007256-200636110-00004

[12] Roberts TJ, Azizi E (2011) Flexible mechanisms: the diverse roles of biological springs in vertebrate movement. J Exp Biol 214(3):353–361. https://doi.org/10.

1242/jeb.038588

[13] de Leva P (1996) Adjustments to Zatsiorsky–Seluyanov's segment inertia parameters. J Biomech 29(9):1223–1230. https://doi.org/10.1016/0021-9290(95)00178-6

[14] Alexander RMcN (1991) Optimum timing of muscle activation for simple models of throwing. J Theor Biol 150(3):349–372. https://doi.org/10.1016/S0022-5193(05)80434-5

[15] Fleisig GS, Nicholls RL, Elliott BC, Escamilla RF (2003) Kinematics used by world class tennis players to produce high-velocity serves. Sports Biomech 2(1):51–64. https://doi.org/10.1080/14763140308522807

[16] Bobbert MF, Gerritsen KGM, Litjens MCA, van Soest AJ (1996) Why is countermovement jump height greater than squat jump height? Med Sci Sports Exerc 28(11):1402–1412. https://doi.org/10.1097/00005768-199611000-00009

[17] Blickhan R (1989) The spring-mass model for running and hopping. J Biomech 22(11–12):1217–1227. https://doi.org/10.1016/0021-9290(89)90224-8

[18] Farley CT, Morgenroth DC (1999) Leg stiffness primarily depends on ankle stiffness during human hopping. J Biomech 32(3):267–273. https://doi.org/10.1016/S0021-9290(98)00170-5

[19] Pandy MG (2001) Computer modeling and simulation of human movement. Annu Rev Biomed Eng 3:245–273. https://doi.org/10.1146/annurev.bioeng.3.1.245

[20] Seth A, Hicks JL, Uchida TK, et al (2018) OpenSim: simulating musculoskeletal dynamics and neuromuscular control to study human and animal movement. PLoS Comput Biol 14(7):e1006223. https://doi.org/10.1371/journal.pcbi.1006223